LUND UNIVERSITY

Temporal and spatial effects inside a compact and CEP stabilized, few-cycle OPCPA system at high repetition rates

Matyschok, Jan; Lang, Tino; Binhammer, Thomas; Prochnow, Oliver; Rausch, Stefan; Schultze, Marcel; Harth, Anne; Rudawski, Piotr; Arnold, Cord; L'Huillier, Anne; Morgner, Uwe

[Link to publication](#)

Temporal and spatial effects inside a compact and CEP stabilized, few-cycle OPCPA system at high repetition rates

Jan Matyschok,[1,2,*] Tino Lang,[1,3] Thomas Binhammer,[2] Oliver Prochnow,[2] Stefan Rausch,[2] Marcel Schultze,[1] Anne Harth,[1,3] Piotr Rudawski,[4] Cord L. Arnold,[4] Anne L'Huillier,[4] and Uwe Morgner[1,3,5]

[1]*Institute of Quantum Optics, Leibniz Universität Hannover, Welfengarten 1, D-30167 Hannover, Germany*
[2]*VENTEON Laser Technologies GmbH, Hertzstraße 1b, D-30827 Garbsen, Germany*
[3]*Centre for Quantum Engineering and Space-Time Research (QUEST), Welfengarten 1, D-30167 Hannover, Germany*
[4]*Department of Physics, Lund University, P.O. Box 118, SE-221 00 Lund, Sweden*
[5]*Laser Zentrum Hannover (LZH), Hollerithallee 8, D-30419 Hannover, Germany*
[*]*matyschok@iqo.uni-hannover.de*

Abstract: We present a compact and ultra-stable few-cycle OPCPA system. In two non-collinear parametric amplification stages pulse energies up to 17 µJ at 200 kHz repetition rate are obtained. Recompression of the broadband pulses down to 6.3 fs is performed with chirped mirrors leading to peak powers above 800 MW. The parametric amplification processes were studied in detail employing (2 + 1) dimensional numerical simulations and compared to experimental observations in terms of spectral shapes, pulse energy, spatial effects as well as delay dependent nonlinear mixing products. This gives new insights into the parametric process and design guidelines for high repetition rate OPCPA systems.

©2013 Optical Society of America

OCIS codes: (190.0190) Nonlinear optics; (190.4410) Nonlinear optics, parametric processes; (190.4970) Parametric oscillators and amplifiers; (320.7090) Ultrafast lasers.

References and links

1. A. Dubietis, R. Butkus, and A. P. Piskarskas, "Trends in chirped pulse optical parametric amplification," IEEE J. Sel. Top. Quantum Electron. **12**(2), 163–172 (2006), http://ieeexplore.ieee.org/stamp/stamp.jsp?tp=&arnumber=1632161&isnumber=34227.
2. G. Cerullo, A. Baltuška, O. D. Mücke, and C. Vozzi, "Few-optical-cycle light pulses with passive carrier-envelope phase stabilization," Laser Photon. Rev. **5**(3), 323–351 (2011), doi:10.1002/lpor.201000013.
3. D. Herrmann, L. Veisz, R. Tautz, F. Tavella, K. Schmid, V. Pervak, and F. Krausz, "Generation of sub-three-cycle, 16 TW light pulses by using noncollinear optical parametric chirped-pulse amplification," Opt. Lett. **34**(16), 2459–2461 (2009), doi:10.1364/OL.34.002459.
4. S. Adachi, N. Ishii, T. Kanai, A. Kosuge, J. Itatani, Y. Kobayashi, D. Yoshitomi, K. Torizuka, and S. Watanabe, "5-fs, multi-mJ, CEP-locked parametric chirped-pulse amplifier pumped by a 450-nm source at 1 kHz," Opt. Express **16**(19), 14341–14352 (2008), doi:10.1364/OE.16.014341.
5. D. Brida, C. Manzoni, G. Cirmi, M. Marangoni, S. Bonora, P. Villoresi, S. De Silvestri, and G. Cerullo, "Few-optical-cycle pulses tunable from the visible to the mid-infrared by optical parametric amplifiers," J. Opt. **12**(1), 013001 (2010), doi:10.1088/2040-8978/12/1/013001.
6. A. Thai, M. Hemmer, P. K. Bates, O. Chalus, and J. Biegert, "Sub-250-mrad, passively carrier-envelope-phase-stable mid-infrared OPCPA source at high repetition rate," Opt. Lett. **36**(19), 3918–3920 (2011), doi:10.1364/OL.36.003918.
7. A. Shirakawa, I. Sakane, M. Takasaka, and T. Kobayashi, "Sub-5-fs visible pulse generation by pulse-front-matched noncollinear optical parametric amplification," Appl. Phys. Lett. **74**(16), 2268 (1999), doi:10.1063/1.123820.
8. A. Harth, M. Schultze, T. Lang, T. Binhammer, S. Rausch, and U. Morgner, "Two-color pumped OPCPA system emitting spectra spanning 1.5 octaves from VIS to NIR," Opt. Express **20**(3), 3076–3081 (2012), doi:10.1364/OE.20.003076.
9. S. Huang, G. Cirmi, J. Moses, K. Hong, S. Bhardwaj, J. R. Birge, L. Chen, E. Li, B. Eggleton, G. Cerullo, and F. X. Kärtner, "High-energy pulse synthesis with sub-cycle waveform control for strong-field physics," Nat. Photonics **5**(8), 475–479 (2011), doi:10.1038/nphoton.2011.140.

10. G. G. Paulus, F. Grasbon, H. Walther, P. Villoresi, M. Nisoli, S. Stagira, E. Priori, and S. De Silvestri, "Absolute-Phase phenomena in photoionization with few-cycle laser pulses," Nature **414**(6860), 182–184 (2001).
11. A. Baltuška, M. Uiberacker, E. Goulielmakis, R. Kienberger, V. S. Yakovlev, T. Udem, T. W. Hänsch, and F. Krausz, "Phase-Controlled Amplification of Few-Cycle Laser Pulses," IEEE J. Sel. Top. Quantum Electron. **9**(4), 972–989 (2003).
12. A. Mikkelsen, J. Schwenke, T. Fordell, G. Luo, K. Klünder, E. Hilner, N. Anttu, A. A. Zakharov, E. Lundgren, J. Mauritsson, J. N. Andersen, H. Q. Xu, and A. L'Huillier, "Photoemission electron microscopy using extreme ultraviolet attosecond pulse trains," Rev. Sci. Instrum. **80**(12), 123703 (2009), doi:10.1063/1.3263759.
13. A. Thai, M. Baudisch, M. Hemmer, and J. Biegert, "20 µJ, few-cycle pulses at 3.1 µm and 160 kHz repetition rate from mid-IR OPCPA," in Conference on Lasers and Electro-Optics 2012, OSA Technical Digest (online) (Optical Society of America, 2012), paper CM1B.2.
14. M. Schultze, T. Binhammer, G. Palmer, M. Emons, T. Lang, and U. Morgner, "Multi-µJ, CEP-stabilized, two-cycle pulses from an OPCPA system with up to 500 kHz repetition rate," Opt. Express **18**(26), 27291–27297 (2010), doi:10.1364/OE.18.027291.
15. J. Rothhardt, S. Demmler, S. Hädrich, J. Limpert, and A. Tünnermann, "Octave-spanning OPCPA system delivering CEP-stable few-cycle pulses and 22 W of average power at 1 MHz repetition rate," Opt. Express **20**(10), 10870–10878 (2012), doi:10.1364/OE.20.010870.
16. J. Rothhardt, S. Demmler, S. Hädrich, T. Peschel, J. Limpert, and A. Tünnermann, "Thermal effects in high average power optical parametric amplifiers," Opt. Lett. **38**(5), 763–765 (2013), doi:10.1364/OL.38.000763.
17. M. Krebs, S. Hädrich, S. Demmler, J. Rothhardt, A. Zaïr, L. Chipperfield, J. Limpert, and A. Tünnermann, "Towards isolated attosecond pulses at megahertz repetition rates," Nat. Photonics **7**(7), 555–559 (2013), doi:10.1038/nphoton.2013.131.
18. A. Vernaleken, J. Weitenberg, T. Sartorius, P. Russbueldt, W. Schneider, S. L. Stebbings, M. F. Kling, P. Hommelhoff, H. D. Hoffmann, R. Poprawe, F. Krausz, T. W. Hänsch, and T. Udem, "Single-pass high-harmonic generation at 20.8 MHz repetition rate," Opt. Lett. **36**(17), 3428–3430 (2011), doi:10.1364/OL.36.003428.
19. C.-T. Chiang, A. Blattermann, M. Huth, J. Kirschner, and W. Widdra, "High-order harmonic generation at 4 MHz as a light source for time-of-flight photoemission spectroscopy," Appl. Phys. Lett. **101**(7), 071116 (2012), doi:10.1063/1.4746264.
20. T. Lang, A. Harth, J. Matyschok, T. Binhammer, M. Schultze, and U. Morgner, "Impact of temporal, spatial and cascaded effects on the pulse formation in ultra-broadband parametric amplifiers," Opt. Express **21**(1), 949–959 (2013), doi:10.1364/OE.21.000949.
21. S. Hädrich, J. Rothhardt, M. Krebs, S. Demmler, J. Limpert, and A. Tünnermann, "Improving carrier-envelope phase stability in optical parametric chirped-pulse amplifiers by control of timing jitter," Opt. Lett. **37**(23), 4910–4912 (2012), doi:10.1364/OL.37.004910.

1. Introduction

In recent years the number of scientific applications requiring intense few-cycle laser pulses with a stable Carrier Envelope Phase (CEP) has rapidly grown. During the last ten years Ti:sapphire-based amplifier systems with subsequent pulse compression stages have been the workhorses especially in the field of High Harmonic Generation (HHG) and attosecond physics. Meanwhile this technique has reached limitations with little potential for further scaling in average power or repetition rate. A lot of effort is presently devoted to the development of the alternative approach of parametric amplifier systems [1, 2]. Optical Parametric Chirped Pulse Amplification (OPCPA) systems are able to directly provide a broad amplification bandwidth and are scalable in terms of output power and repetition rate. Direct amplification of few-cycle laser pulses into the mJ-regime [3, 4] has been shown in a variety of wavelength regimes from the visible to the mid-infrared [5–7]. Combining several Optical Parametric Amplifier (OPA) stages, even the single cycle limit comes within reach and pulse durations well below 5 fs have been demonstrated [8, 9]. The CEP of few-cycle pulses is an important parameter for applications such as photoionization [10] or HHG [11], and furthermore many experimental applications (e.g. photoemission electron microscopy [12]) will benefit from a higher repetition rate due to shorter integration times, higher photon flux, and increased statistics. In the range from 100 kHz up to 1 MHz some multi-µJ systems have been reported [13, 14], emitting up to 22 W of average power with elaborate laboratory set-ups [15]. Although in principle thermal effects are negligible in OPA based systems, absorption of the infrared idler or multi-photon absorption can lead to limitations of average power [16]. CEP-stable few-cycle OPCPA systems operated above 100 kHz have recently been used successfully for HHG into the cutoff regions [17] showing the potential of this technology. Even lower energies in the µJ range have been shown to be sufficient for HHG with few-cycle pulses [18, 19]. As experiments for XUV and attosecond spectroscopy are

getting more and more complex, there is a strong need for reliable, long-term stable, and user-friendly light sources.

In this paper we present a compact OPCPA system at 200 kHz repetition rate which is able to deliver CEP-stable few-cycle pulses with high peak power. The setup is designed for maximum compactness, low complexity, and low noise in order to bring the OPCPA technology to the next step towards compact and reliable light sources, ideally suited for many types of nonlinear light-matter interaction experiments. The easy and robust setup provides excellent noise performance and CEP stability with pulse durations as shot as 6.3 fs. A CEP stabilized octave-spanning seed oscillator provides the ultra-broadband signal and the narrowband seed for the Yb-based pump amplifier without further nonlinear spectral shifting. After two subsequent Non-collinear Optical Parametric Amplifier (NOPA) stages up to 17 µJ of pulse energy is demonstrated. The NOPA design in the case of high pulse repetition rates with moderate pump energies requires tight focal spot sizes and comparably large crystal lengths for efficient parametric amplification. Therefore, the influence of spatial as well as walk-off effects has to be taken carefully into account. To investigate various experimentally observed spatial phenomena occurring along with the NOPA in the chosen Poynting-Vector-Walk-off Compensation (PVWC) geometry we used our $(2 + 1)$ dimensional propagation simulation code [20]. Temporal, spatial, and cascaded effects were investigated and compared to the experimental results. Additionally the influence of the temporal delay between signal and pump pulse in the OPA to the spatially observed nonlinear mixing products are examined. These features might be useful for future novel stabilization schemes (see e.g [21].). The remarkable agreement between simulation and experimental results increases the confidence in the $(2 + 1)$ dimensional approximation which can provide vital support for designing future OPCPA systems.

2. Experimental setup

An overview of the experimental setup of the OPCPA system is given in Fig. 1. It consists of a CEP stabilized broadband Ti:sapphire oscillator, and an ytterbium doped fiber preamplifier seeding two separate rod-type fiber amplifiers which are operated in parallel. After pulse compression and Second Harmonic Generation (SHG), they individually pump the two parametric amplifier stages which are followed by a chirped mirror compressor and an f-to-2f interferometer. The whole system fits on a compact footprint (150 x 210 cm) and is boxed for low amplitude and CEP noise. The Ti:sapphire oscillator (VENTEON | PULSE: ONE OPCPA SEED) delivers an octave spanning spectrum from 600 nm – 1200 nm with an average output power of 240 mW at 80 MHz. The outer edges of this spectrum are filtered and sent into a self-referencing f-to-2f interferometer for CEP stabilization. The feedback to the oscillator is implemented by pump power modulation via an acousto-optic modulator, whereas slow drifts are corrected by moving the intra-cavity wedge pair by a motorized stage. This way, a low rms phase noise of 80 mrad (3 Hz – 1 MHz) and a long-term locking for more than 12 hours can be achieved. After filtering for CEP locking, more than 90% of the output power is still available. A dichroic filter extracts the long wavelength part, centered at 1030 nm, from the oscillator spectrum to seed the fiber amplifier. Due to the large fundamental bandwidth, no external spectral shifting in e.g. nonlinear fibers is required to reach the fiber amplification band with sufficient seed energy of more than 40 pJ, which greatly enhances the noise performance and long-term stability of the amplifier seed. In addition, no coupling or soliton effects are affecting the timing jitter between pump and signal pulses of the OPCPA, which is especially important when using pump pulses below 1 ps. The main spectral region from 650 nm – 1020 nm, which still supports sub-6 fs pulses, with 2.5 nJ of pulse energy is used as signal radiation for the subsequent NOPA stages.
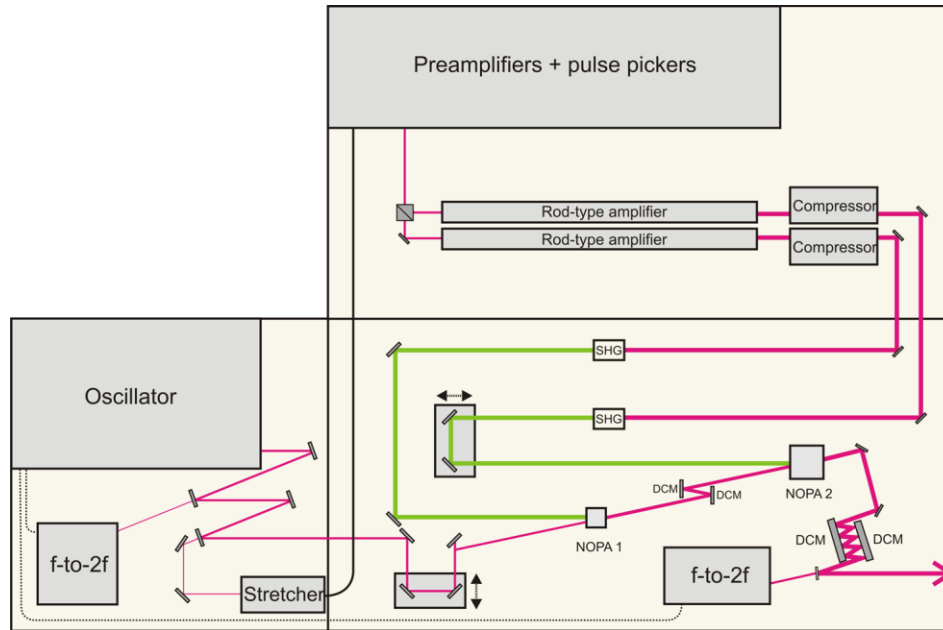
Fig. 1. Experimental setup of the OPCPA system: SHG: Second Harmonic Generation; NOPA: Non-collinear Optical Parametric Amplifier; DCM: Double Chirped Mirrors; f-to-2f: interferometer for the carrier envelope phase measurement.

Before coupling into the three-stage fiber preamplifier which includes two pulse pickers, the infrared light centered at 1030 nm is spectrally filtered and temporally stretched by a Chirped Volume Bragg Grating (CVBG, 27 ps/nm, 16 nm FWHM) with an efficiency of 75%. The advantages of this approach are the monolithic and thereby drift-free design and the small footprint of the stretcher arrangement, which can be implemented within the oscillator housing. After preamplification to about 300 mW at 200 kHz repetition, the output of the preamplifier is divided into two beam lines for seeding two independent 80 cm long rod-type fibers (NKT, DC 285/100 PM-Yb-ROD) for power amplification. The advantages of this parallel approach are the reduced pulse energy and average power in each main amplification stage compared to a one-stage amplifier, and the possibility to optimize the pump pulse energies and pulse durations for the NOPA stages independently. The fiber main amplifiers deliver an average power of 20 W for the first and 23 W for the second amplification stage before compression. Nevertheless, the stretched pump pulse duration obtained from the CVBG limits the pulse energy in the fiber amplifier due to nonlinear effects. While in the present implementation the focus was on compactness and reduced complexity of the stretcher unit, further energy scaling could therefore be realized in the future by implementing a different stretching concept, e.g. with a much less compact and stable grating sequences. Pulse compression is optimized to maximum parametric yield and performed by a second CVBG matched to the stretcher with an efficiency of 57% (first stage) and by a GRISM with 67% efficiency (second stage). The GRISM was used instead of a designated third CVBG due to the higher efficiency together with the better pulse and beam quality. After frequency doubling, pump energies of 27 µJ are available for the first stage and 44 µJ for the second stage, with pulse durations of around 500 fs as derived from the measured intensity autocorrelations of the compressed infrared pulses.

Parametric amplification of the seed pulses takes place in two BBO crystals whereby broadband phase matching is achieved by non-collinear interaction of pump and signal beam in the crystals. For the first parametric amplification stage, the temporal overlap of signal and pump pulses are controlled by a translation stage, while the pulse duration of the broadband Ti:sapphire signal is adapted to the pump pulse duration. Subsequently, the chirp of the signal

pulse is reduced with chirped mirrors to optimize the pulse duration for optimum temporal overlap in the second BBO crystal. After both NOPA stages, a chirped mirror compressor with more than 80% efficiency is used to compress the pulses down to the final pulse duration.

3. Experimental results

In the first NOPA the pump beam is focused down to a $1/e^2$-beam radius of 175 μm and temporally and spatially overlapped with the signal which exhibits a slightly smaller radius of 110 μm. The angle between signal and pump corresponds to 2.4° to achieve the most broadband phase matching. For the given pump energy, the PVWC geometry was chosen with a crystal length of 5 mm. Amplification from 1.25 nJ (at 80 MHz) up to 4.5 μJ (at 200 kHz) was achieved. Due to the temporal stretching of the broadband signal in glass, air and BBO, the pulse duration after the first stage is stretched to 420 fs (measured with SPIDER). The positive chirp of the seed is slightly reduced using two bounces on a chirped mirror pair (VENTEON, 600-1200 nm, -120 fs^2 / pair at 800 nm).

The second NOPA is operated with the same crystal parameters with approximately 270 fs input pulse duration and 3.4 μJ pulse energy of the signal. The input beam is focused down to 170 μm radius. For the pump, with energy of 44 μJ, a slightly larger spot size of 270 μm was chosen to keep the intensity on the BBO crystal below 100 GW/cm^2 to avoid crystal damages. Here, amplification up to 17 μJ is achieved, corresponding to an optical-to-optical power conversion efficiency of 31% from pump to signal. The spectral bandwidth after the second NOPA spans more than 450 nm (at -10 dBc) (see Fig. 2(a)) and supports a pulse duration of 4.9 fs. Due to short pump pulses and corresponding moderate stretching, pulse compression with a chirped mirror compressor is possible. The simple, compact, and drift-free compressor uses 12 reflections in double-pass configuration and shows an overall throughput above 80%. The mirror dispersion is designed for compensation of the BBO crystal, air, and fused silica. The pulse duration after compression is measured as 6.3 fs (see Fig. 2(b)) using a commercial SPIDER system (VENTEON | PULSE: FOUR SPIDER).
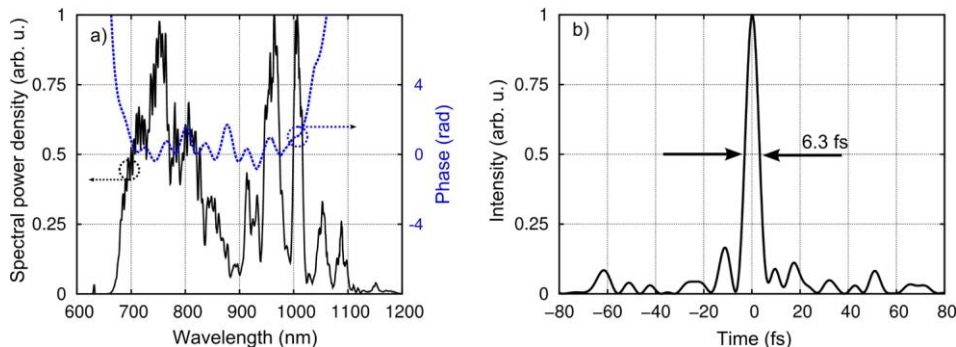

Fig. 2. a) Measured spectrum from the compressed pulse after the second NOPA stage (black) together with the spectral phase (dotted blue) from the SPIDER measurement. b) Reconstructed pulse from the SPIDER measurement.

After pulse compression, a small fraction of the beam (approx. 300 nJ) is separated and sent to an f-to-2f interferometer. The interference pattern (see Fig. 3(a); approx. 4000 spectra from an USB-spectrometer, Avantes AVASPEC-2048-USB2) allows to determine directly the CEP. With a slow feedback loop for thermal drift compensation, an excellent stability of 68 mrad over 15 min could be reached (see Fig. 3(b)), showing the high intrinsic stability of the compact system.

The low noise of the fiber-based amplifier in combination with a low timing jitter between signal and pump pulses result in high stability of the average output power which is measured to be below 0.5% over 100 min after a certain warm up time. CEP and power stability measurements are performed without any active delay stabilization. This intrinsic stability

was obtained by the optical synchronization between signal and pump pulse, the single pass pump amplification, the completely boxed and compact setup in combination with water cooling at several points of the system to enhance the thermal stability.
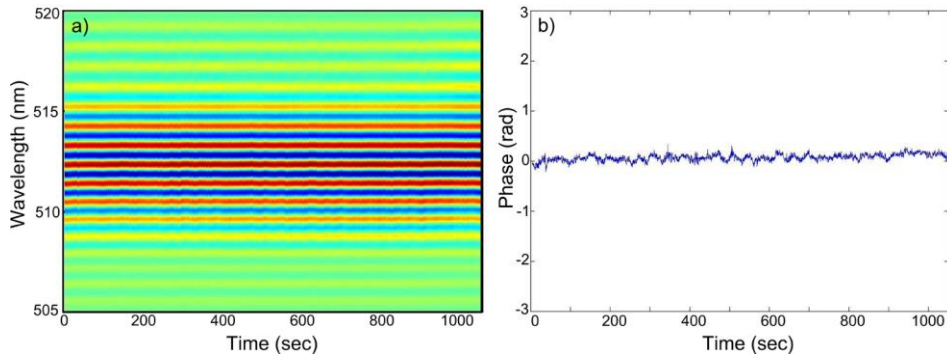

Fig. 3. a) Interference pattern measured with the f-to-2f interferometer after the second parametric amplification stage and the chirped mirror compressor controlled with the second feedback loop. The spectra were recorded with 3 ms integration time and an average over 10 spectra respectively. b) Phase of the fringe pattern given in Fig. 3(a) corresponding to an rms noise < 70 mrad.

The combination of µJ-level energy with high repetition rate and few-cycle pulses with excellent CEP stability makes this system an ideal source for high-intensity applications such as ionization or HHG.

4. Numerical simulations and spatial effects

For a better understanding of the temporal and spatial effects during the parametric amplification, we performed extensive numerical modeling of the amplification process including two spatial as well as the time dimension. This simulation is based on solving the linear and nonlinear propagation equations for the ordinary and extraordinary polarized waves. The spatial behavior is treated in two dimensions in order to describe the non-collinear propagation, including phase matching, as well as walk-off and focusing/diffraction effects. Further details about the numeric are given in a previous publication [20]. The parameters for the simulation of the two amplification stages, such as spot sizes, pump energies, and pulse durations are taken from the experiment. The seeding signal field for the first NOPA was taken from the measured spectral amplitude and phase from the Ti:sapphire oscillator. The phase matching angle Θ can be precisely chosen to reproduce the experimental situation e.g. via the spectral position of the distinctive dip caused by the parasitic SHG. The non-collinear angle α between signal and pump as well as the delay between both pulses are adapted in the simulation to reproduce the experimentally observed spectrum.

A comparison between the experimental results and the results from the simulation are shown in Fig. 4(a). For angles $\Theta = 24.35°$ and $\alpha = 2.43°$, the spectral structures as well as the spectral bandwidth match very well the experimental results. For a quantitative extraction of pulse energies from the calculations, radial symmetry of the beam is assumed, and the signal beam radius is taken to be the measured one. For 27 µJ of pump energy, an amplification from 1.25 nJ to 4.4 µJ is calculated which is very close to the 4.1 µJ obtained in the experiment. The energy slopes from simulation and experiment are compared in Fig. 4(b). Again the simulation is capable to predict the output of the OPCPA stage with high accuracy.

The results from the first NOPA together with the dispersion of the chirped mirrors in between both stages are used as input with the measured beam sizes for modeling the second amplification stage. For the second stage $\Theta = 24.2°$ and $\alpha = 2.36°$ lead to the best match between experimental and simulated spectra with optimized temporal delay (see Fig. 4(a)). The simulation is able to reproduce the spectral shape and bandwidth of the signal. Also for

the second amplification stage, the signal vs. pump energy slope is comparable to the measurement (see Fig. 4(b)).
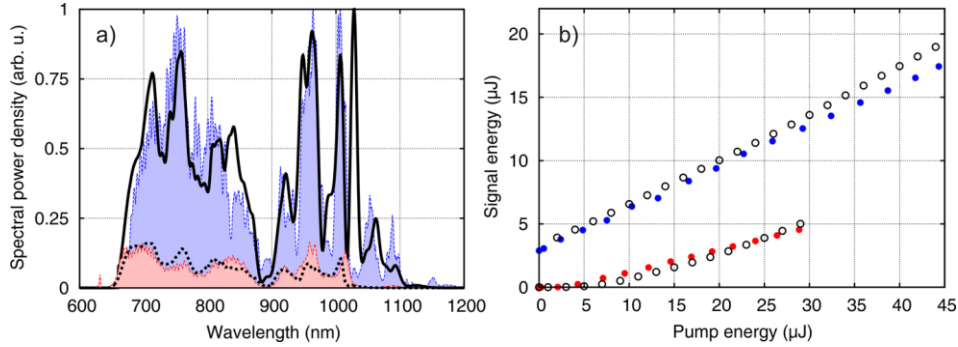

Fig. 4. a) Measured spectra obtained from the first (shadowed red) and second (shadowed blue) NOPA stage together with the calculated spectra from the numerical simulation of the first (dashed line) and second (black line) NOPA. b) Measured (red first NOPA, blue second NOPA) and calculated (black circles) pulse energy after each amplification stage for different pump energies.

The agreement between the simulation and experiment prove the correctness of the algorithm and allows for predicting the performance of the OPCPA in different situations. This is especially helpful in finding optimum beam waists for signal and pump or comparing both Tangential Phase Matching (TPM) and PVWC geometry with respect to efficiency, beam profile, and compressibility. The numerical model indicates that with 27 μJ of pump energy a crystal length of 5 mm is required to reach a conversion efficiency of > 10%. For such crystal lengths the PVWC geometry is preferable due to better compressibility around 650 nm. Furthermore, in TPM there is a strong angular deviation from the collimated signal beam in this spectral region which leads to a distorted beam profile of the signal. This spatial distortion makes the TPM geometry less favorable for the chosen crystal length and given pump energies.

Since the model predicts the angular distributions of signal and idler beams as well as of all other phase matched mixing products, we are able – for the first time to our knowledge – to perform a direct comparison between experiment and simulations of the non-collinear parametric process including spatial angle distribution and delay dependence including all mixing products. This provides unprecedented insight into the different processes. In Fig. 5, the simulated angle and frequency distribution of the first parametric amplification stage in the chosen PWVC geometry is shown. For experimental access, a screen with a hole for the intense pump beam is placed behind the first parametric amplification stage, and the angular distribution for several delays is recorded with a digital camera (Nikon D300, see inset Fig. 5 and Fig. 6(c)). The angle axes of these pictures are rescaled to the propagation angles inside the nonlinear crystal by compensating for the BBO surface refraction.

The transversal spatial dimension of the model is indicated as the central line (CL) of the photograph (see inset Fig. 5 marked with white dots). The other dimension of the image belongs to the third spatial dimension which is not included in the simulation. Identification of the observed features in Fig. 5 can be easily done in the model by turning on and off the different nonlinear effects and the separate consideration of the ordinary (o) and extraordinary (e) polarization within the simulation. The feature (A, e) around alpha = 0° is attributed to the intensive pump at 515 nm (0.58 PHz) not visible on the photo due to the hole in the screen. At $\alpha = 2.5°$ the broadband amplified signal spanning from 0.27 PHz to 0.46 PHz (B, o) with the likewise phase matched parasitic SHG to 0.68 PHz (C, e) is visible in the simulated data corresponding to a bright white signal spot in the photograph from the experiment. Due to energy and momentum conservation the corresponding idler is generated in the infrared between 0.12 PHz and 0.33 PHz and spatially dispersed between $\alpha = -2.5°$ to $-10°$ (D, o). This idler wave is broadband phase matched for a SHG process, which leads to the bright

green to red feature in the visible wavelength region between −2.5° and −5° (E, e). The predicted colors and angles from the simulation fit well with the observations from the experiment.
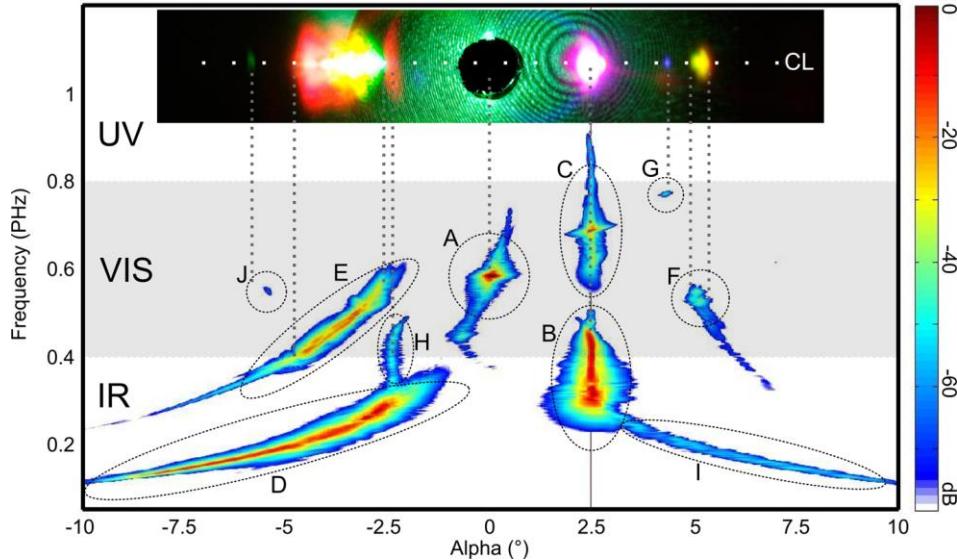

Fig. 5. Results of the numerical model with the parameters from the first parametric amplification stage. For comparison the visible wavelength range are shaded. The picture shows the 515 nm pump (feature A) at alpha = 0°, the broadband seed (between 0.27 - 0.46 PHz, B) with the parasitic SHG at 0.7 PHz (C). Also visible is the spectral dispersive idler wave in the infrared (IR) region (D) at negative angles with frequency doubling to the visible (VIS) region (E) together with further mixing products in the visible (F, G, J). The inset shows a photograph taken from a screen behind the first BBO crystal with a hole for the pump light.

Apart from these well-known beams also a few other mixing products show up in good agreement with experimental observations; now, their origin can be identified: **i)** The visible feature at α = 5.1° (F, o) is explained by a simultaneously phase matched DFG process where the parasitic SHG (C) around 0.68 PHz of the signal (B) at α = 2.5° serves as pump radiation and the infrared idler (D) around −6.8° as seeded idler. The extension from feature (F) to larger angles and lower frequencies is following the corresponding phase matching curve. **ii)** A phase matched SFG process of the part of feature (F) around 5.4° and 0.48 PHz with the infrared part of the signal (B) around 0.29 PHz and 2.5° leads to the small blue spot (G, e) visible at 4.3°. **iii)** The red feature (H, o) located next to the SHG of the idler at α = −2.5° can be explained as super-fluorescence and occurs in the simulation only by adding white noise resulting in a signal following the phase matching curve with the corresponding infrared idler (I, o) at positive angles between 2.5° and 10°. **iv)** No clear explanation has been found for the tiny green spot (J, e) around −5.4° which occurs in both experiment and simulation with a slight angular offset. The offset can be attributed to the re-scaling of the photograph (see Fig. 5 inset and Fig. 6(c)) to match the internal angles, where the difference between ordinary and extraordinary refractive index was neglected. Furthermore the change of the refractive index for the different propagation angles in the extraordinary polarization was neglected in the conversion from the spatial frequencies used in the simulation to the propagation angles in Fig. 5 and Fig. 6(a).

In Fig. 6 the temporal delay between signal and pump was changed between −500 and + 600 fs in steps of 67 fs, and for each delay the angular intensity distribution was determined by integration over the visible spectral region (shaded area in Fig. 5). The results are shown in Fig. 6(a) and compared to a series of photographs as in Fig. 5. The zero position of the delay axis is chosen to match the simulation. In the simulation, zero delay means signal and pump

pulse ideally overlapping in time at the beginning of the crystal. Positive delay means that the signal is ahead of the pump pulse. Due to the different dispersion properties of ordinary and extraordinary propagation, a delay of around + 200 fs leads to the optimum amplification. By integration over the three color channels from the central line of each photograph shown in Fig. 6(c), a more quantitative representation of the angular distribution can be extracted (see Fig. 6(b)). Due to saturation/nonlinear response of the photo camera sensor, no robust statements concerning relative intensities can be extracted, but still the overall agreement is quite remarkable; several mixing products only appear around the optimal delay where signal and idler are most broadband and intense. At large negative delays, the super-fluorescence signal at $\alpha = -2.5°$ is most prominent and almost vanishes at the ideal delay. The green spot at $\alpha = -6°$ also shows a strong delay dependence, and is only present in a range of + 100 fs up to + 600 fs.
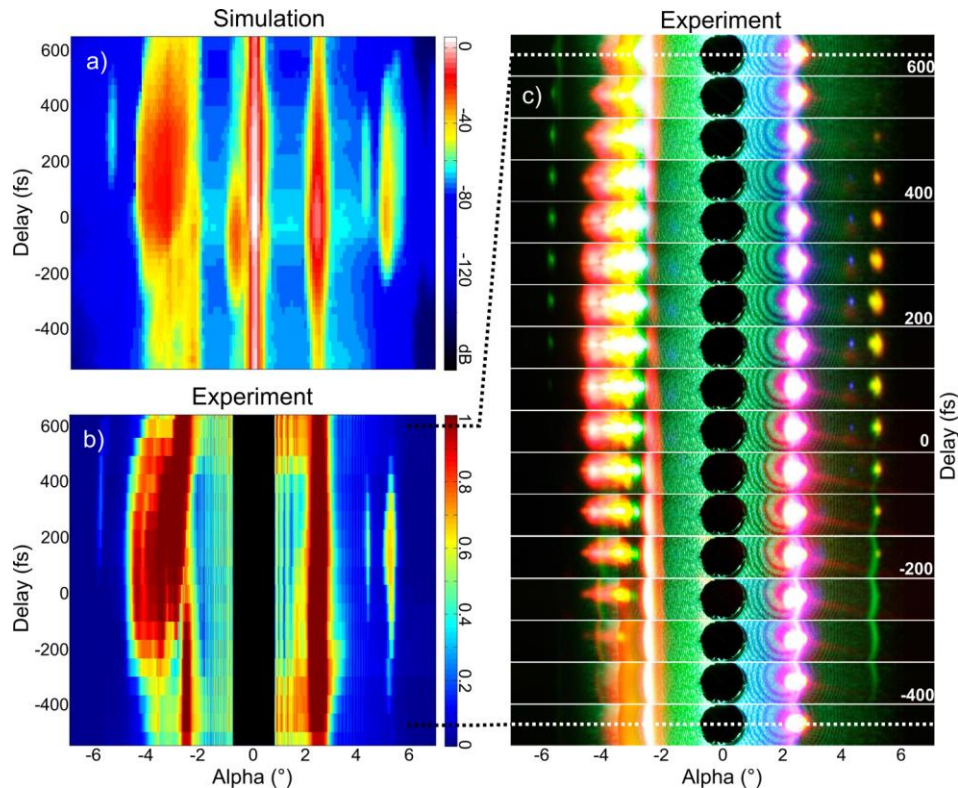

Fig. 6. a) Integration over the spatial power distribution of the visible wavelength range given from the results of the numerical simulation of the first amplification stage as a function of the relative delay between signal and pump. b) Shows the evaluation of the photographs from the experiment (given in 6c) taken from the experiment after the first parametric amplification stage with delay variation in steps of 67 fs between signal and pump.

The spatially and temporally resolved analysis presented here can be easily extended to the TPM geometry. There, it has been shown in [21], that some mixing products can be successfully used for stabilization of the relative delay or the CEP of the amplifier output. For the PVWC geometry, so far no nonlinear mixing product usable for CEP stabilization has been identified. Delay stabilization can be most easily done by detecting the spectral wings of the second harmonic of the idler which show an opposite dependence on delay for the high and low frequency edges (see Fig. 6(b)). Figure 6 reveals even more delay dependent signals, but their usability for stabilization has to be further investigated.

5. Conclusion

In this work an OPCPA system with high repetition rate and few-cycle CEP-stable pulses has been presented. Energies of more than 10 μJ have been generated with high conversion efficiency. Due to the compact and robust system design, low noise below 0.5% rms for the output power and below 70 mrad for the CE phase error could be obtained. The system is thus ideally suited for applications requiring high peak power such as HHG or photoionization. Further up-scaling of the system is possible by extending the stretching of the pump pulses into the ns-regime. For the given pump energy of 27 μJ for the first and 44 μJ for the second pump stage, 5 mm long BBO crystals and relatively small focal sizes are required for high conversion efficiencies. In this case the PVWC geometry is favorable. Extensive numerical simulations with the model from [20] show a remarkable agreement with the experimental observations. Both, angular distributions as well as the energy scaling curves are well predicted. A complete comparison of the numerically calculated and experimentally observed angular distribution of all phase matched nonlinear mixing products within the parametric process has been presented. The investigation of the delay dependence of the observed signals might lead to useful delay or CEP stabilization schemes.

The agreement between experiment and simulation reveals the potential of the model to establish design criteria for future short pulse OPCPA systems. As the simulation is easily adapted to different nonlinear crystals and wavelength ranges, it allows for novel insights into phase matching conditions and the expected nonlinear mixing products while providing the best geometry and focal sizes for the respective experimental parameters. This is especially important for high repetition rate OPCPA systems with limited pump energy, smaller focal sizes, and longer crystals. The analysis emphasizes the importance of spatial effects and gives some novel insight into the colorful and rich physics involved in the nonlinear process.

Acknowledgments